Letter | Editors' Suggestion

Tilt-driven antiferroelectricity in $PbZrO_3$

Konstantin Shapovalov [1,*] and Massimiliano Stengel [2,1]
[1]Institut de Ciència de Materials de Barcelona (ICMAB-CSIC), Campus UAB, 08193 Bellaterra, Spain
[2]ICREA—Institució Catalana de Recerca i Estudis Avançats, 08010 Barcelona, Spain

(Received 22 December 2021; revised 9 March 2023; accepted 1 June 2023; published 12 July 2023)

Antiferroelectricity is a state of matter that has so far eluded a clear-cut definition. Even in the best-known material realization, $PbZrO_3$, the physical nature of the driving force towards an antipolar order has not been settled yet. Here, by building a Landau-like continuum Hamiltonian from first principles via an exact long-wave approach, we reconcile the existing theories in terms of a single physical mechanism. In particular, we find that a formerly overlooked trilinear coupling between tilts, tilt gradients, and polarization provides a surprisingly accurate description of the energetics and structure of the antiferroelectric ground state of $PbZrO_3$. We discuss the relevance of our findings to other ferrielectric and incommensurate polar structures that were recently observed in perovskites.

DOI: 10.1103/PhysRevMaterials.7.L071401

Antiferroelectric (AFE) materials have received increasing attention recently, both for their potential applications (e.g., in energy storage) and for their fundamental interest [1–4]. $PbZrO_3$ (PZO) is by far the best-studied example, and yet a theoretical understanding of this material has so far proven to be elusive [5–10]. During its AFE phase transition at ∼500 K, PZO changes its crystalline symmetry from cubic $Pm\bar{3}m$ to orthorhombic *Pbam*, with Pb ions forming the ↑↑↓↓ pattern periodically repeated in a ⟨110⟩ direction [Fig. 1(a)]. This phase transition is accompanied by additional nontrivial atomic distortions, including antiferrodistortive (AFD) O_6 octahedra tilts [5,6,8], whose relationship to the antipolar pattern is not well understood. Several models have been proposed to explain the physical origin of antiferroelectricity in PZO.

In the first major model, Tagantsev *et al.* [5] rationalize AFE as a manifestation of an incommensurate (IC) phase transition driven by flexoelectricity. Flexoelectricity, describing the coupling between electrical polarization and strain gradients [11–14], enters the continuum bulk Hamiltonian via a Lifshitz invariant, which can stabilize modulated phases if the coupling is sufficiently strong [5,15,16]. If, moreover, the optimal period of the modulation is close to a multiple of the cell parameter, it can spontaneously lock into a commensurate phase [17], which would explain [5] the ↑↑↓↓ AFE pattern of Pb displacements in PZO. This idea appears to be very reasonable: IC phases have indeed been reported in PZO [18] and closely related perovskites [9,19,20]. However, there are conflicting experimental reports on whether flexoelectricity is strong enough for such a mechanism to be viable [5,21]. Moreover, flexoelectricity alone does not explain the simultaneous condensation of the AFD octahedral tilt mode, whose amplitude and contribution to the energetics are remarkably large in the ground-state structure [6,22].

The second model, proposed by Íñiguez *et al.* [6], invokes a trilinear coupling between the antipolar displacement of the Pb atoms [a Σ-point distortion with wave vector $\mathbf{q}_\Sigma = (1/4, 1/4, 0)$], the AFD octahedra tilt mode [*R*-point, $\mathbf{q}_R = (1/2, 1/2, 1/2)$], and a third *S*-point mode [$\mathbf{q}_S = (1/4, 1/4, 1/2)$]. Such Σ–*R*–*S* interaction would lower the energy when the three modes coexist and hence explain their simultaneous condensation. Their first-principles-based parametrization confirms that this coupling is indeed essential for the *Pbam* structure to win over competing low-energy phases [6]. The main conceptual issue is that Σ or *S* phonons can hardly be regarded as "elementary fields" in the theoretical study of perovskite materials: Both of them correspond to complex distortion patterns, whose physical interpretation is (especially in the case of the *S* mode) unclear. In other words, these modes are specific to the ground-state structure of PZO, so their physical properties appear difficult to generalize to other systems where the antipolar ordering occurs with different symmetries and/or periodicities [9,22].

Here we develop a unified theoretical framework that merges the two models into a single physical mechanism. In particular, we show that the transition is driven by a trilinear coupling term that is akin to flexoelectricity but involves gradients of the AFD octahedral tilt modes, rather than of the strain. Couplings of such symmetry are ubiquitous in the physics of (multi)ferroics, their effects ranging from the generation of polarity at the twin boundaries in $SrTiO_3$ [23] to polar textures in inversion-symmetry-broken magnets [24]; this and similar mechanisms have been discussed in the context of IC and AFE phases [7,25]. Thus our interpretation saves the idea of an incommensurate phase transition, while endowing the *S* mode with a clear physical interpretation as a modulated tilt mode. By establishing an exact mapping between continuum theory and first-principles simulations in the long-wavelength limit, we validate the continuum approach, qualitatively and quantitatively reproducing the energetics and structure of the ground-state AFE structure within our model.

*Corresponding author: shapovalov.kos@gmail.com

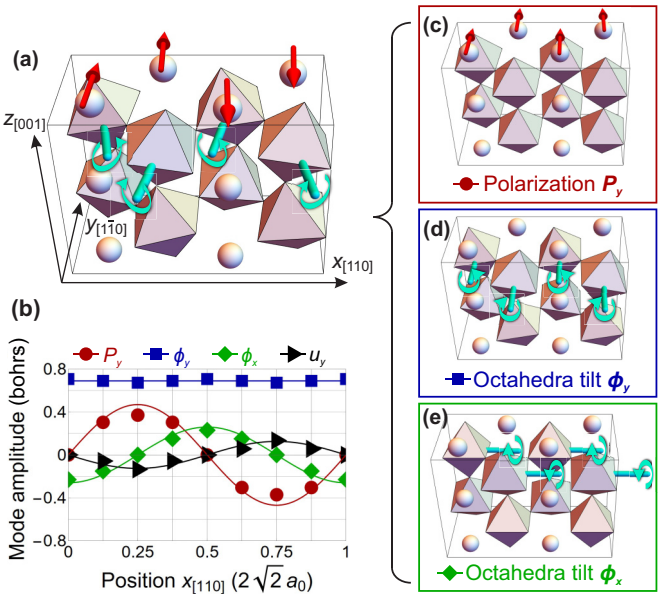

FIG. 1. (a) Calculated atomic structure of the *Pbam* phase of PZO. Only Pb atoms (spheres) and O_6 octahedra are shown. Red arrows indicate polar displacements of Pb atoms, and blue arrows indicate O_6 octahedra tilts. (b) Decomposition of the atomic distortions shown in (a) over polarization P_y, AFD octahedral tilts ϕ_x, ϕ_y, and displacement field u_y. Symbols and solid lines correspond to the layer-by-layer and Fourier decompositions, respectively. One bohr of amplitude corresponds to 174 μC/cm^2 of polarization and 14.8° of octahedral tilt. (c)–(e) Atomic distortions described by the three primary order parameters (P_y, ϕ_y, ϕ_x).

Our results provide the missing link required for triggering the IC phase transition in PZO and related materials and can be regarded as a universal pathway towards incommensuration in ferroics.

Structural analysis. In order to discuss the emergence of modulated phases, we need first of all to establish a rigorous mapping between spatially inhomogeneous order parameters and the atomic structure of PZO. Following earlier works [23,26], we identify the order parameters with the eigenvectors of the force-constant matrix calculated *ab initio* at high-symmetry points of the parent $Pm\bar{3}m$ Brillouin zone (see Supplemental Material Sec. S1 [27] and Refs. [28–30] therein for the details of the density functional theory (DFT) calculations). More specifically, we consider the following two types of distortions: (i) zone-center modes, including the "soft" polar mode (**P**) and the acoustic branch (**u**), and (ii) out-of-phase AFD tilts of the oxygen octahedra (***ϕ***), located at the *R* point of the cubic phase. To extract the continuum fields from a given atomic distortion pattern, we then operate either in Fourier space [via a decomposition into **q** points of the $Pm\bar{3}m$ Brillouin zone and a subsequent projection onto the basis of distortion (i) or (ii)] or in real space (by constructing, starting from the cell-periodic patterns of distortion (i) or (ii), a space-resolved basis of "local modes" centered on (110) layers; see Supplemental Material Sec. S2 [27] for details). In the following we test both approaches on the first-principles-calculated *Pbam* phase of PZO [Fig. 1(a)] and check their mutual consistency.

Our Fourier decomposition shows, in agreement with previous studies [6,8], that the $\mathbf{q_R}$, $\mathbf{q_\Sigma}$, and $\mathbf{q_S}$ modes of the *Pbam* phase account for 63.0, 33.2, and 3.8%, respectively, of the total distortion. In Fig. 1(b) we show the spatially resolved order parameters, plotted as functions of the x coordinate (x corresponds to the [110] modulation direction, and y corresponds to the antipolar displacement of the Pb atoms along $[1\bar{1}0]$; see Fig. 1(a)). Both the layer-by-layer approach and the Fourier approach result in similar field amplitudes, confirming that our analysis is physically sound. The largest distortion corresponds to a uniform AFD mode with the tilt axis oriented along y, ϕ_y [Fig. 1(d)], accounting for the near totality (99.8%) of the *R* mode. Next, we identify a sinusoidal modulation of the polarization, P_y [Fig. 1(c)], which reflects the characteristic ↑↑↓↓ antiferroelectric displacement of the Pb ions and constitutes the largest (92.0%) contribution to the Σ mode. The remainder of the Σ distortion is predominantly due to the acoustic mode, u_y, whose amplitude describes the local displacement of the unit cell along y. Finally, and most importantly, our analysis reveals a *secondary* tilt mode, ϕ_x [Fig. 1(e)], which has not been reported before. This mode has the tilt axis oriented along x (longitudinal) and is modulated with the same period as the polarization, its phase shifted by 90° [Fig. 1(b)]. A closer look shows that this modulated tilt coincides to a high accuracy (92.9%) with the *S* mode that was reported in the literature [6]. Together, the four modes plotted in Fig. 1(b) amount to 99.0% of the total distortion amplitude.

The above analysis unambiguously identifies the main distortions of the *Pbam* phase, including the "exotic" Σ and *S* modes of the standard decomposition, as spatial modulations of polar and tilt modes. This constitutes a drastic conceptual simplification, since it allows us to describe a structure as complex as the AFE ground state of PZO in terms of "elementary" fields that are ubiquitous in perovskite materials. It presents practical advantages, too: In combination with recent developments in first-principles theory [13,23,26,31,32] that enable systematic calculation of gradient-mediated couplings, the aforementioned mapping between lattice modes and continuum fields allows for a quantitative (i.e., free of fitted parameters or phenomenological assumptions) validation of the physical mechanisms that were proposed so far as the driving force towards the antiferroelectric state.

Flexoelectricity. In general, the gradient coupling between a strain ε and a polar mode P can be written as

$$E_{\mathrm{fxe}} = -fP\frac{\partial \varepsilon}{\partial x}, \tag{1}$$

where f is the flexoelectric coupling coefficient [12,14,26]. This expression is typically discussed in conjunction with the standard Landau-Ginzburg-Devonshire (LGD) free energy of a ferroelectric, which in its simplest form contains the homogeneous Landau potential $E_{\mathrm{hom}}(P) = AP^2/2 + BP^4/4$, the correlation energy $E_{\mathrm{corr}}(P) = G(\partial P/\partial x)^2/2$, and the elastic energy $E_{\mathrm{elas}}(\varepsilon) = C\varepsilon^2/2$ [12]. A strong flexoelectric coupling may trigger a transition to a modulated phase if the following criterion is satisfied [5,15]:

$$G^* = G - \frac{f^2}{C} < 0, \tag{2}$$

where G^* is the renormalized correlation coefficient after imposing the stationary condition on the strain [12]. Whenever

Eq. (2) holds, domain walls can spontaneously form, making the homogeneous ferroelectric phase unstable; thus G^* can be regarded as a useful indicator of the proximity to the unstable regime. To check whether Eq. (2) is satisfied in PZO, we extract the relevant modulation-direction-dependent material parameters from first principles via a perturbative expansion of the energy around the cubic phase with respect to *both* phonon mode amplitudes and wave vector $\hat{\mathbf{q}}$ [32] (see Supplemental Material Sec. S1 [27] for details) and obtain the full anisotropic $G^*(\hat{\mathbf{q}})$ dependence. We find the absolute minimum of $G^*(\hat{\mathbf{q}})$ at $\hat{\mathbf{q}} = \langle 110 \rangle$, 82% smaller than its maximum at $\hat{\mathbf{q}} = \langle 100 \rangle$, which matches well the modulation direction of the observed *Pbam* structure. However, though G^* is significantly smaller than in other well-known perovskites such as $BaTiO_3$ and $SrTiO_3$ (see Supplemental Material Sec. S5 [27] and Refs. [23,26,33] therein), it is still positive, meaning that a modulated state cannot form spontaneously in PZO due to flexoelectricity alone.

Rotopolar coupling. There are other Lifshitz-like invariants that are allowed by symmetry in perovskites [25]: for example, the "rotopolar" coupling [23], whereby gradients of the AFD tilt modes, rather than of the elastic strain, couple to the polarization. In the context of the *Pbam* phase of PZO, such coupling can be written as

$$E_{\mathrm{rp}} = -W P_y \phi_y \frac{\partial \phi_x}{\partial x}. \tag{3}$$

This means that in the presence of a uniform transverse tilt (ϕ_y), the gradient of the transverse polarization (P_y) couples to the longitudinal tilt (ϕ_x) and vice versa. This fits nicely with the physical picture that emerges from Fig. 1(b): Both the observed 90° phase shift between the two modulated modes (a feature of an IC phase transition driven by *gradient* couplings [16]) and the Cartesian components of the distortions are consistent with Eq. (3). For a quantitative assessment, we extract the numerical value of W from first principles by following the same procedure as in Ref. [23], i.e., by taking the long-wavelength limit of the third-order force constants within the cubic reference structure (see Supplemental Material Sec. S1 [27] and Ref. [34] therein for details). Similar to G^*, the stationary condition on $\varepsilon_6 = \partial u_y/\partial x$ leads to the renormalization of the rotopolar coefficient, $W^* = W + fR/C$, where R quantifies the rotostrictive coupling, $E_{\mathrm{rs}} = -R\phi_x\phi_y\varepsilon_6$; see Supplemental Material Sec. S4 [27] for details. We find that W^* in PZO is about as large as in $SrTiO_3$; its anisotropy analysis gives the absolute maximum of $W^*(\hat{\mathbf{q}})$ along $\langle 110 \rangle$, 2.3 times stronger than $W^*(\langle 100 \rangle)$ (see Supplemental Material Sec. S5 [27] and Refs. [23,26,33] therein), consistent with the geometry of the AFE ground state.

As can be seen from Eq. (3), E_{rp} is manifestly a *trilinear* function of the mode amplitudes, which suggests some close connection to the model of Ref. [6]. Indeed, as we identified above, Σ-, R-, and S-point distortions are largely composed of, respectively, $P_y = Q_\Sigma \cos(qx)$, $\phi_y = Q_R$, and $\phi_x = Q_S \sin(qx)$, where $q = \pi/(\sqrt{2}a_0)$ is the modulation wave vector and a_0 is the lattice constant of the cubic unit cell. Using this in Eq. (3), we obtain $\langle E_{\mathrm{rp}} \rangle = -(W^* q/2) Q_\Sigma Q_R Q_S$, thus recovering the trilinear Σ–R–S coupling described in Ref. [6]. After converting to the unit conventions of Ref. [6], we obtain a coupling energy between Σ, R, and S modes amounting to 63.3 meV per five-atom formula unit (f.u.); this compares well with their reported value of 48.4 meV/f.u.

TABLE I. Energies of various phases in PZO compared with the cubic $Pm\bar{3}m$ structure in meV/f.u., with lattice parameters constrained to the $Pm\bar{3}m$ phase values.

Structure	Phase	DFT	Landau
Imcm	uniform $\boldsymbol{\phi}\|\|\langle 110 \rangle$	−226	−226
Ima2	uniform $\mathbf{P}$, $\boldsymbol{\phi}\|\|\langle 110 \rangle$	−257	−259
R3c	uniform $\mathbf{P}$, $\boldsymbol{\phi}\|\|\langle 111 \rangle$	−275	−275
FiE	modulated $\mathbf{P}$, $\boldsymbol{\phi}\|\|\langle 110 \rangle$	−273	−265
Pbam	modulated $\mathbf{P}$, $\boldsymbol{\phi}\|\|\langle 110 \rangle$	−269	−273
$4\uparrow 4\downarrow$	modulated $\mathbf{P}$, $\boldsymbol{\phi}\|\|\langle 110 \rangle$	−263	−268

Continuum functional. To make the above arguments more quantitative, we construct an LGD functional that incorporates the main physical ingredients discussed so far (see Supplemental Material Secs. S3 and S4 and Ref. [35] therein for details),

$$F = F^*_{\mathrm{hom}}(\mathbf{P}, \boldsymbol{\phi}) + \frac{1}{2}G^*\left(\frac{\partial P_y}{\partial x}\right)^2 + \frac{1}{2}D_{11}\left(\frac{\partial \phi_x}{\partial x}\right)^2 + \frac{1}{2}D_{66}\left(\frac{\partial \phi_y}{\partial x}\right)^2 - W^* P_y \phi_y \frac{\partial \phi_x}{\partial x}. \tag{4}$$

Here, $F^*_{\mathrm{hom}}(\mathbf{P}, \boldsymbol{\phi})$ is the eighth-order expansion with respect to homogeneous $\mathbf{P}$ and $\boldsymbol{\phi}$, obtained via a least-squares fitting to the first-principles energy landscape of PZO at the $Pm\bar{3}m$ lattice parameters (the fixed-strain approach is justified for the purposes of this Research Letter, which will be shown below); its description of the metastable nonmodulated phases observed *ab initio* is essentially exact (<3 meV/f.u.; see Table I and Supplemental Material Sec. S3 [27]). The remaining terms in Eq. (4) are specific to the *Pbam* and other modulated phases of PZO, defined by the correlation coefficients for the polarization (G^*), for the longitudinal (D_{11}) and the transverse (D_{66}) tilts, and by the rotopolar coupling (W^*).

Minimization of Eq. (4) via numerical finite-element methods yields a locally stable modulated phase whose energy (−273 meV/f.u.) and equilibrium structure [see Fig. 2(a)] accurately reproduce our DFT simulations of the AFE *Pbam* phase. Moreover, the optimal period of modulations following from our Landau potential lies within 5% from the experimentally observed $2\sqrt{2}a_0$ [Figs. 2(a) and 2(b)], which supports the umklapp lock-in mechanism [17] that was proposed in earlier works [5]. The overall agreement between the DFT and continuum description of the *Pbam* phase is exceptional, given the fact that the modulations occur on the scale of a few unit cells, i.e., in a regime where the continuum approximation is usually regarded as unreliable. We emphasize that such a close correspondence was obtained by constructing the Landau potential of Eq. (4) via a series of well-defined approximations to the reference DFT model (i.e., by taking a rigorous long-wave limit of the low-energy Hamiltonian) and without introducing any phenomenological fitting parameter to the gradient terms.

By its nature, rotopolar coupling is not limited to the *Pbam* phase, but is of high relevance in the whole range of modulated structures. To show this, we have performed

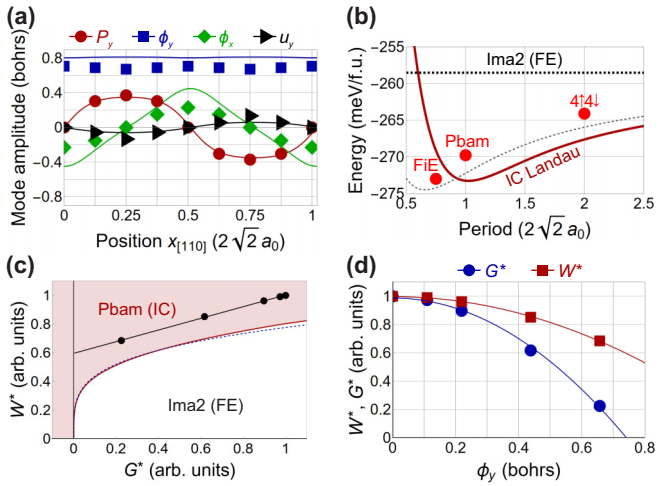

FIG. 2. (a) Spatial distribution of polarization P_y, AFD tilts ϕ_x, ϕ_y, and displacement field u_y in the IC *Pbam* phase described by Eq. (4) (solid lines), compared with the layer-by-layer decomposition shown in Fig. 1(b) (symbols). One bohr of amplitude corresponds to 174 μC/cm^2 of polarization and 14.8° of octahedral tilt. (b) Energy of the IC *Pbam* phase at different periods of modulations described by Eq. (4) with gradient coefficients extracted in the $Pm\bar{3}m$ phase (red solid line) and in the presence of a $\phi_y = 0.7$ bohr distortion (gray dashed line), compared with the energies of the FE *Ima*2 phase (black dotted line) and of the modulated phases observed *ab initio* (red circles). (c) Phase diagram between the *Pbam* (red region) and *Ima*2 (white region) phases described by Eq. (4) at varying correlation G^* and rotopolar W^* coefficients. The blue dashed line follows the analytical expression in Eq. (5). The black symbols and line correspond to the ones shown in (d). (d) G^* and W^* coefficients extracted from DFT at varying frozen uniform tilt ϕ_y (symbols), and their quadratic fits (solid lines).

additional *ab initio* and Landau-based analysis of the ↑↑↓ ferrielectric (FiE) structure, which has recently been described theoretically [10] and observed experimentally [36], and of the "four-up–four-down" (4 ↑ 4 ↓) modulated phase having modulation period twice as large as in *Pbam* (Table I). For the FiE phase, the first-principles calculations show strong structural similarities with the ↑↑↓↓ *Pbam* phase, including uniform transverse and modulated longitudinal AFD tilts (see Supplemental Material Sec. S7 [27]), allowing its treatment as a modulated phase. Our continuum theory matches well the *ab initio* energies of the three modulated phases (Table I), though the energy-vs-period curve [red solid line in Fig. 2(b)] is shifted towards larger modulation periods compared with the first-principles data points. Note that our description of modulated phases is not merely theoretical: The available x-ray data on the *real* IC structures (e.g., in $PbHfO_3$ [37], a closely related perovskite) show all the features discussed in this Research Letter, including the modulated longitudinal tilts; see Supplemental Material Sec. S7 [27] for details.

Stability analysis. To formalize the role of the gradient couplings in the formation of modulated structures, we study the stability of the ferroelectric (FE) *Ima*2 phase against an IC transition as a function of the main physical parameters at play, W^* and G^*. *Ima*2, characterized by ⟨110⟩-oriented uniform polarization and AFD tilts, is essentially the modulationless "parent phase" of *Pbam*; therefore the *Pbam–Ima*2 phase diagram will provide the *necessary* condition for the IC phase to exist. Note that strain relaxation (which is not included in our model potential) plays virtually no role in this context: Our *ab initio* calculations show that FE *Ima*2, AFE *Pbam*, and FiE phases gain the same amount of energy at elastic equilibrium compared with the $Pm\bar{3}m$ lattice parameters, −6 to −7 meV/f.u. Figure 2(c) shows the *Pbam–Ima*2 phase boundary (red solid line) emerging from our direct study of the *Pbam* phase energetics via minimization of Eq. (4) with respect to the order parameters and periodicity.

In the small-G^* regime, the condition for the IC instability of *Ima*2 is well described [blue dashed line in Fig. 2(c)] by

$$\gamma(\phi_{y0}W^*)^4 > D_{11}G^*, \tag{5}$$

where ϕ_{y0} is the spontaneous tilt of the *Ima*2 phase and $\gamma \sim 1/[(\partial^2 F^*_{\rm hom}/\partial P_y^2)(\partial^2 F^*_{\rm hom}/\partial \phi_x^2)]$ is a well-defined "softness" parameter (see Supplemental Material Sec. S6 [27] for its exact expression and derivation). Equation (5) generalizes the classic criterion for the IC phase formation shown in Eq. (2), recovering it for vanishing ϕ_{y0} or W^*. The calculated G^* and W^* coefficients clearly satisfy Eq. (5) in PZO [the (1,1) point in Fig. 2(c)], consistent with the conclusions that we have reached via numerical minimization of Eq. (4).

A potential limitation of our approach consists in having calculated G^* and W^* in the $Pm\bar{3}m$ reference structure. This raises the obvious question of whether the (large) uniform O_6 tilts may modify the value of such coefficients, possibly affecting the stability regime. To verify such a possibility, we have recalculated both coefficients several times in the presence of a ϕ_y distortion of increasing amplitude, ranging from zero to the ground-state value of Fig. 1(b). The results, plotted in Fig. 2(d), show a significant decrease of both coefficients for increasing ϕ_y. Remarkably, after plotting $G^*(\phi_y)$ and $W^*(\phi_y)$ in Fig. 2(c), the resulting line lies well within the unstable region of the phase diagram, meaning that the ϕ_y dependence of these coefficients, not taken into account in our Landau potential, is largely irrelevant for the tendency towards a modulated state. At the same time, using the coefficients extracted at $\phi_y = 0.7$ bohr in our potential [Eq. (4)] gives a closer match of the optimal periodicity of the IC phase [gray dashed line in Fig. 2(b)].

It is interesting to note that G^* in Fig. 2(d) transitions to negative values for tilt amplitudes that are only slightly larger than our calculated ϕ_{y0}. Such a critical behavior suggests that the antiferroelectric state of PZO may, in fact, originate from a *triggered* IC transition [governed, at leading order in ϕ_y, by $E_{\rm tr} = K\phi_y^2(\partial P_y/\partial x)^2$], thus questioning the necessity of the rotopolar mechanism that we propose here. (Note that this same coupling term, $E_{\rm tr}$, was proposed recently as a driving force towards incommensuration in closely related materials [38].) To confirm the role of the rotopolar mechanism in the *Pbam* phase formation, we have performed constrained-DFT relaxations where the secondary tilt ϕ_x (and hence the rotopolar coupling) is suppressed by hand. This can be done cleanly as the modulated ϕ_x distortion has a different symmetry compared with the other active modes in the system. The energy of the resulting AFE *Pbam*-like structure is −256 meV/f.u., i.e., slightly higher than *Ima*2, meaning that there is no driving force towards incommensuration in the absence of the rotopolar coupling, consistent with Fig. 2(c). This

result conclusively demonstrates the *necessity* of the rotopolar coupling for stabilizing the AFE state in PZO, making it the prime candidate for the "missing" mechanism alluded to in Ref. [5].

Discussion and outlook. To conclude, we have validated the continuum theory approach for the description of the AFE, FiE, and other modulated structures of $PbZrO_3$ and have demonstrated the crucial role played by the trilinear gradient *rotopolar* coupling between polarization and antiferrodistortive tilts in the stabilization of modulated structures in tilted perovskites. We can further speculate that either the rotopolar mechanism or such higher-order couplings may be involved in the formation of the recently discussed *Pnma*–80 phase [39,40] (the additional distortions take indeed the form of two-dimensional modulated polarization and tilts), and thereby we provide a unified framework to explain the emergence of spatially modulated structure in tilted perovskites. Application of these ideas to the many examples that have been recently discussed in the literature [9,19,40,41] constitutes, in our view, an exciting avenue for further study.

Acknowledgments. We acknowledge the support of Ministerio de Ciencia e Innovación (MCIN/AEI/10.13039/501100011033) through Grant No. PID2019-108573GB-C22 and the Severo Ochoa FUNFUTURE Centre of Excellence (CEX2019-000917-S) and of Generalitat de Catalunya (Grant No. 2017 SGR1506). This project has received funding from the European Research Council (ERC) under the European Union's Horizon 2020 research and innovation program (Grant Agreement No. 724529). Part of the calculations were performed at the Supercomputing Center of Galicia (CESGA). We thank Philippe Ghosez for useful discussions and Roman Burkovsky for reading through the manuscript and providing input regarding the text.

[1] K. M. Rabe, Antiferroelectricity in oxides: A reexamination, in *Functional Metal Oxides* (Wiley, New York, 2013), Chap. 7, pp. 221–244.

[2] X. Hao, J. Zhai, L. B. Kong, and Z. Xu, A comprehensive review on the progress of lead zirconate-based antiferroelectric materials, Prog. Mater. Sci. **63**, 1 (2014).

[3] X.-K. Wei, A. K. Tagantsev, A. Kvasov, K. Roleder, C.-L. Jia, and N. Setter, Ferroelectric translational antiphase boundaries in nonpolar materials, Nat. Commun. **5**, 3031 (2014).

[4] B. Xu, J. Íñiguez, and L. Bellaiche, Designing lead-free antiferroelectrics for energy storage, Nat. Commun. **8**, 15682 (2017).

[5] A. K. Tagantsev, K. Vaideeswaran, S. B. Vakhrushev, A. V. Filimonov, R. G. Burkovsky, A. Shaganov, D. Andronikova, A. I. Rudskoy, A. Q. R. Baron, H. Uchiyama, D. Chernyshov, A. Bosak, Z. Ujma, K. Roleder, A. Majchrowski, J.-H. Ko, and N. Setter, The origin of antiferroelectricity in $PbZrO_3$, Nat. Commun. **4**, 2229 (2013).

[6] J. Íñiguez, M. Stengel, S. Prosandeev, and L. Bellaiche, First-principles study of the multimode antiferroelectric transition in $PbZrO_3$, Phys. Rev. B **90**, 220103(R) (2014).

[7] J. Hlinka, T. Ostapchuk, E. Buixaderas, C. Kadlec, P. Kuzel, I. Gregora, J. Kroupa, M. Savinov, A. Klic, J. Drahokoupil, I. Etxebarria, and J. Dec, Multiple Soft-Mode Vibrations of Lead Zirconate, Phys. Rev. Lett. **112**, 197601 (2014).

[8] B. Xu, O. Hellman, and L. Bellaiche, Order-disorder transition in the prototypical antiferroelectric $PbZrO_3$, Phys. Rev. B **100**, 020102(R) (2019).

[9] Z. Fu, X. Chen, Z. Li, T. Hu, L. Zhang, P. Lu, S. Zhang, G. Wang, X. Dong, and F. Xu, Unveiling the ferrielectric nature of $PbZrO_3$-based antiferroelectric materials, Nat. Commun. **11**, 3809 (2020).

[10] H. Aramberri, C. Cazorla, M. Stengel, and J. Íñiguez, On the possibility that $PbZrO_3$ not be antiferroelectric, npj Comput. Mater. **7**, 196 (2021).

[11] P. Zubko, G. Catalan, and A. K. Tagantsev, Flexoelectric effect in solids, Annu. Rev. Mater. Res. **43**, 387 (2013).

[12] P. V. Yudin and A. K. Tagantsev, Fundamentals of flexoelectricity in solids, Nanotechnology **24**, 432001 (2013).

[13] M. Stengel and D. Vanderbilt, First-principles theory of flexoelectricity, in *Flexoelectricity in Solids: From Theory to Applications*, edited by A. K. Tagantsev and P. V. Yudin (World Scientific, Singapore, 2016), Chap. 2, pp. 31–110.

[14] B. Wang, Y. Gu, S. Zhang, and L.-Q. Chen, Flexoelectricity in solids: Progress, challenges, and perspectives, Prog. Mater. Sci. **106**, 100570 (2019).

[15] J. D. Axe, J. Harada, and G. Shirane, Anomalous acoustic dispersion in centrosymmetric crystals with soft optic phonons, Phys. Rev. B **1**, 1227 (1970).

[16] H. Pöttker and E. K. H. Salje, Flexoelectricity, incommensurate phases and the Lifshitz point, J. Phys.: Condens. Matter **28**, 075902 (2016).

[17] P. Bak, Commensurate phases, incommensurate phases and the devil's staircase, Rep. Prog. Phys. **45**, 587 (1982).

[18] R. G. Burkovsky, I. Bronwald, D. Andronikova, B. Wehinger, M. Krisch, J. Jacobs, D. Gambetti, K. Roleder, A. Majchrowski, A. V. Filimonov, A. I. Rudskoy, S. B. Vakhrushev, and A. K. Tagantsev, Critical scattering and incommensurate phase transition in antiferroelectric $PbZrO_3$ under pressure, Sci. Rep. **7**, 41512 (2017).

[19] A. Bosak, V. Svitlyk, A. Arakcheeva, R. Burkovsky, V. Diadkin, K. Roleder, and D. Chernyshov, Incommensurate crystal structure of $PbHfO_3$, Acta Crystallogr. Sect. B: Struct. Sci. Cryst. Eng. Mater. **76**, 7 (2020).

[20] T. Ma, Z. Fan, B. Xu, T.-H. Kim, P. Lu, L. Bellaiche, M. J. Kramer, X. Tan, and L. Zhou, Uncompensated Polarization in Incommensurate Modulations of Perovskite Antiferroelectrics, Phys. Rev. Lett. **123**, 217602 (2019).

[21] P. Vales-Castro, K. Roleder, L. Zhao, J.-F. Li, D. Kajewski, and G. Catalan, Flexoelectricity in antiferroelectrics, Appl. Phys. Lett. **113**, 132903 (2018).

[22] R. G. Burkovsky, I. Bronwald, D. Andronikova, G. Lityagin, J. Piecha, S.-M. Souliou, A. Majchrowski, A. Filimonov, A. Rudskoy, K. Roleder, A. Bosak, and A. Tagantsev, Triggered incommensurate transition in $PbHfO_3$, Phys. Rev. B **100**, 014107 (2019).

[23] A. Schiaffino and M. Stengel, Macroscopic Polarization from Antiferrodistortive Cycloids in Ferroelastic $SrTiO_3$, Phys. Rev. Lett. **119**, 137601 (2017).

[24] M. Mostovoy, Ferroelectricity in Spiral Magnets, Phys. Rev. Lett. **96**, 067601 (2006).

[25] E. A. Eliseev, S. V. Kalinin, Y. Gu, M. D. Glinchuk, V. Khist, A. Borisevich, V. Gopalan, L.-Q. Chen, and A. N. Morozovska, Universal emergence of spatially modulated structures induced by flexoantiferrodistortive coupling in multiferroics, Phys. Rev. B **88**, 224105 (2013).

[26] M. Stengel, Unified *ab initio* formulation of flexoelectricity and strain-gradient elasticity, Phys. Rev. B **93**, 245107 (2016).

[27] See Supplemental Material at http://link.aps.org/supplemental/10.1103/PhysRevMaterials.7.L071401 for details of first-principles calculations, real-space mapping between atomic distortions and continuum fields, Landau energy, anisotropy of G^*, W^* in $PbZrO_3$ and other perovskites, analytical expression for the *Ima*2–*Pbam* phase diagram, examples of modulated phases in perovskites.

[28] X. Gonze, B. Amadon, P.-M. Anglade, J.-M. Beuken, F. Bottin, P. Boulanger, F. Bruneval, D. Caliste, R. Caracas, M. Côté, T. Deutsch, L. Genovese, Ph. Ghosez, M. Giantomassi, S. Goedecker, D. R. Hamann, P. Hermet, F. Jollet, G. Jomard, S. Leroux *et al.*, ABINIT: First-principles approach to material and nanosystem properties, Comput. Phys. Commun. **180**, 2582 (2009).

[29] X. Gonze, B. Amadon, G. Antonius, F. Arnardi, L. Baguet, J.-M. Beuken, J. Bieder, F. Bottin, J. Bouchet, E. Bousquet, N. Brouwer, F. Bruneval, G. Brunin, T. Cavignac, J.-B. Charraud, W. Chen, M. Côté, S. Cottenier, J. Denier, G. Geneste *et al.*, The ABINIT project: Impact, environment and recent developments, Comput. Phys. Commun. **248**, 107042 (2020).

[30] A. H. Romero, D. C. Allan, B. Amadon, G. Antonius, T. Applencourt, L. Baguet, J. Bieder, F. Bottin, J. Bouchet, E. Bousquet, F. Bruneval, G. Brunin, D. Caliste, M. Côté, J. Denier, C. Dreyer, P. Ghosez, M. Giantomassi, Y. Gillet, O. Gingras *et al.*, ABINIT: Overview and focus on selected capabilities, J. Chem. Phys. **152**, 124102 (2020).

[31] M. Stengel, Flexoelectricity from density-functional perturbation theory, Phys. Rev. B **88**, 174106 (2013).

[32] M. Royo and M. Stengel, First-Principles Theory of Spatial Dispersion: Dynamical Quadrupoles and Flexoelectricity, Phys. Rev. X **9**, 021050 (2019).

[33] A. Zabalo and M. Stengel, Switching a Polar Metal via Strain Gradients, Phys. Rev. Lett. **126**, 127601 (2021).

[34] D. R. Hamann, Optimized norm-conserving Vanderbilt pseudopotentials, Phys. Rev. B **88**, 085117 (2013).

[35] L. Bellaiche and J. Íñiguez, Universal collaborative couplings between oxygen-octahedral rotations and antiferroelectric distortions in perovskites, Phys. Rev. B **88**, 014104 (2013).

[36] R.-J. Jiang, Y. Cao, W.-R. Geng, M.-X. Zhu, Y.-L. Tang, Y.-L. Zhu, Y. Wang, F. Gong, S.-Z. Liu, Y.-T. Chen, J. Liu, N. Liu, J.-H. Wang, X.-D. Lv, S.-J. Chen, and X.-L. Ma, Atomic insight into the successive antiferroelectric–ferroelectric phase transition in antiferroelectric oxides, Nano Lett. **23**, 1522 (2023).

[37] H. Fujishita, K. Kato, E. Nishibori, M. Takata, M. Sakata, and S. Katano, Structural modulations in the intermediate phase of antiferroelectric $PbHfO_3$, J. Phys. Soc. Jpn. **87**, 124603 (2018).

[38] M. A. Kniazeva, A. E. Ganzha, I. Jankowska-Sumara, M. Paściak, A. Majchrowski, A. V. Filimonov, A. I. Rudskoy, K. Roleder, and R. G. Burkovsky, Ferroelectric to incommensurate fluctuations crossover in $PbHfO_3-PbSnO_3$, Phys. Rev. B **105**, 014101 (2022).

[39] J. S. Baker, M. Paściak, J. K. Shenton, P. Vales-Castro, B. Xu, J. Hlinka, P. Márton, R. G. Burkovsky, G. Catalan, A. M. Glazer, and D. R. Bowler, A re-examination of antiferroelectric $PbZrO_3$ and $PbHfO_3$: An 80-atom *Pnam* structure, arXiv:2102.08856 [cond-mat.mtrl-sci].

[40] B. F. Grosso and N. A. Spaldin, Prediction of low-energy phases of $BiFeo_3$ with large unit cells and complex tilts beyond glazer notation, Phys. Rev. Mater. **5**, 054403 (2021).

[41] J.-W. Kim, P. Thompson, S. Brown, P. S. Normile, J. A. Schlueter, A. Shkabko, A. Weidenkaff, and P. J. Ryan, Emergent Superstructural Dynamic Order due to Competing Antiferroelectric and Antiferrodistortive Instabilities in Bulk $EuTiO_3$, Phys. Rev. Lett. **110**, 027201 (2013).